Replication of micro/nano scale features by micro injection molding with Bulk Metallic Glass (BMG) mold insert

N Zhang[1], J S Chu[1,2] C J Byrne[1], D J Browne[1] and M D Gilchrist[1*]

[1]School of Mechanical and Materials Engineering, University College Dublin, Ireland
[2] Micromolding Solutions Inc, Boucherville, Greater Montreal, QC, Canada

*: Correspondence to: michael.gilchrist@ucd.ie

Abstract. The development of MEMS and Microsystems needs a reliable mass production process to fabricate micro components with micro/nano scale features. In our study, we used the micro injection molding process to replicate micro/nano scale channels and ridges from a Bulk Metallic Glass (BMG) cavity insert. High density polyethylene (HDPE) was used as the molding material and Design of Experiment (DOE) was adopted to systematically and statistically investigate the relationship between machine parameters, real process conditions and replication quality. The peak cavity pressure and temperature were selected as process characteristic values to describe the real process conditions that material experienced during the filling process. The experiments revealed that the replication of ridges, including feature edge, profile and filling height, was sensitive to the flow direction; cavity pressure and temperature both increased with holding pressure and mold temperature; replication quality can be improved by increasing cavity pressure and temperature within a certain range. The replication quality of micro/nano features is tightly related to the thermomechanical history of material experienced during the molding process. In addition, the longevity and roughness of the BMG insert was also evaluated based on the number of injection molding cycles.

1. Introduction

The development of MEMS and Microsystems (MST) is inspiring the global trend towards miniaturization, which is creating a huge market for micro components with micro/nano scale features [1], especially microfluidic devices, which have wide applications in chemical, biological and medical diagnostics, etc [2]. Currently, the dimensions of micro channels for microfluidic devices range from 10 to 100 μm and even extend to the submicron and nanometer scale for manipulation and measurement of individual molecules [3-5]. Nanophotonic, super hydrophobic surfaces and optical gratings are all macro in scale, but they all have surface features in micro/nano scale [6-8]. Therefore, a mass production process with high replication accuracy needs to be developed for such devices. Polymer is the most promising material for both MEMS and Microsystems, due to its low cost, available fabrication technologies and wide range of mechanical and optical properties and chemical

resistances, etc [9]. On the basis of conventional injection molding technology, micro injection molding has demonstrated itself to be a key enabling fabrication technology for mass production of polymer micro components with complex shapes and products with high quality surface features, e.g. micro fluidic devices [10].

However, because of the high surface to volume ratio of micro/nano features, especially for higher aspect ratios, earlier solidification of polymer melts will prevent the filling of micro/nano cavities. Therefore, high injection pressure and material temperature are required to avoid premature solidification. As a result, the polymer materials in micro injection molding are subject to higher shear rates and thermal gradients than in conventional injection molding. Unique morphological features and lower mechanical properties than those reported for conventional parts have been reported for micro injection molding [11]. It is also reported that the quality of micro components is very sensitive to process variations [12]. Thus, it is very important to understand the thermomechanical history that materials experience during the micro injection molding process. However, because of limited space available to install sensors into the cavity of a micro part, it is difficult to investigate the actual process conditions of micro injection process [13]. In the present study, the micro injection molding process was characterized using embedded pressure and temperature sensors. A reliable and repeatable micro injection molding process to replicate micro/nano scale features, such as micro channels and ridges, is proposed on the basis of our investigation of the relationship between machine parameters, process conditions, and replication quality.

The replication of micro/nano scale features also poses challenges for the tooling technologies and a durable master mold with well fabricated micro/nano scale features will be critical for mass production with the micro injection molding process. The traditional silicon-based molds are brittle and have a limited longevity [6, 14, 15]. Metal, such as nickel stamper, has been widely used as micro/nano scale molds [8]. However, this requires electrodeposition of nickel which is a slow and expensive process, and nickel shim is also thin and very flexible. Although metal molds are stronger than semiconductors, the patterning of metals on the nano-scale is limited by their finite grain size [16]. Bulk metallic glasses exhibit superior mechanical properties and are intrinsically free from grain size limitations and are gradually being applied to research of micro/nano scale molding, such as hot embossing [16-19] and micro injection molding [20, 21]. In addition to its appealing mechanical properties, BMG can be easily used for precision thermal plastic forming at length scale spanning from ~10nm to 10cm [22-24]. Therefore, it can facilitate requirements for manufacturing over different length scales [25]. In our previous work, we characterized the muti-scale machining capability with of BMG with Focused Ion Beam from 10^{-5}m to 10^{-7}m and extended its application to nanometer scale injection molding as mold tools [26].

In the present work, we characterize the replication micro/nano scale features from a BMG mold insert with the micro injection molding process. In addition, we used pressure and temperature sensors embedded into a micro cavity to monitor the cavity pressure and temperature that the material experienced in the molding process. We also systematically investigated the correlations between machine parameter settings, process conditions and the replication quality of features. The influences of flow direction and channel width on the replication quality of micro/nano features were studied under the optimized combination of process parameters obtained from the correlation study. The performance of BMG material after approximately 10000 and 20000 injection molding cycles was also evaluated.

2. Experimental methods

2.1 Machine, mold and material

All the experiments were implemented using a Fanuc Roboshot S-2000i 15B reciprocating micro injection molding machine. The mold was manufactured according to the specified requirements of this study, as shown in figure 1 (a). The mold cavity was formed by a steel mold insert with an embedded BMG insert on the top, as displayed in figure 1 (b). The BMG rods were fabricated with a drop-casting technique in an inert environment and its

composition was Zr47Cu45Al8. These rods were then cut into short lengths via a high-speed diamond saw, and the circular faces were then ground and polished. BMG die inserts were machined from the castings, via micro-EDM (Electro-Discharge Milling), and incorporated into a die-set for micro-injection molding. The surface of the BMG tool was polished to an average surface roughness of ~170nm. The molded part is around 25.34mm^3 in volume with a designed cavity thickness of 0.5mm, as shown in figure 1 (c). The detailed dimensions are displayed in figure 1 (d).

A FEI Quanta 3D FEG Dual Beam FIB was used to machine the sub-micron and nano scale features on the surface of the BMG insert. As shown in figure 2 (a), four groups of micro/nano features were milled near the shoulder of the dog-bone part as shown in figure 1(d). Two groups are channels and the other two groups are ridges, which have been arranged parallel to and against the flow direction, as seen in figure 2 (a). The depth of channels on BMG is 2.24 µm with standard deviation of 0.07µm. The designed widths ranged from 4 µm to 0.3 µm. The height of ridges is 1.91 µm with standard deviation of 0.14µm with designed widths from 4 µm to 0.45 µm respectively. The logo of University College Dublin (UCD) was also machined as a nanostructured surface on the BMG insert, as shown in figure 2 (b).

High density polyethylene (HDPE HMA016 grade) was selected as the molding material because of its wide processing window and excellent processability with good impact strength and dimensional stability.

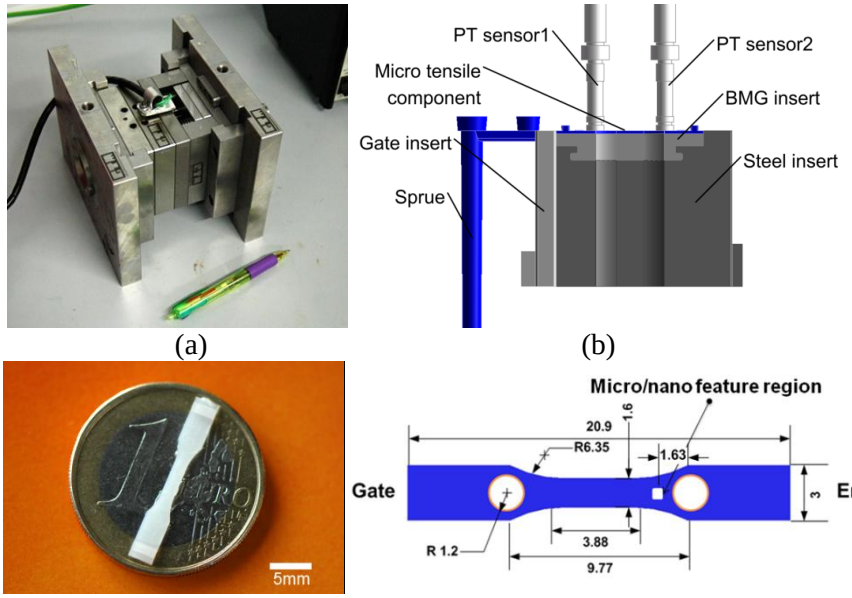

(a) (b) (c) (d)

Figure1. Mold and molded part: (a) entire mold, (b) bulk metallic glass insert, (c) HDPE molded micro component, (d) dimensions of molded part (all in mm).

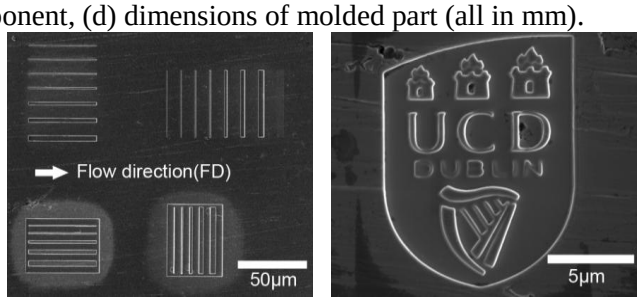

(a) (b)

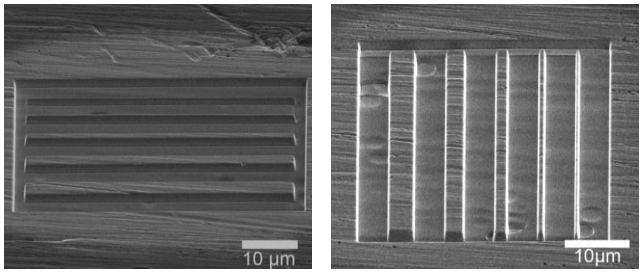

(c) (d)

Figure 2. Micro/nano features on BMG: (a) channel and ridge features, (b) logo of UCD, (c) ridges along flow direction, (d) ridges against flow direction.

2.2 Data acquisition system

A Kistler CoMo injection process monitoring system (2869B) was used for process monitoring and data acquisition. A Kistler 6189A combined pressure and temperature sensor was adapted to measure cavity pressure and material contact temperature at the same position, as shown in figure 1 (b). The cavity pressure and material contact temperature were firstly collected by the CoMo and then were outputted into a computer by Ethernet. The injection signals from the injection molding machine were used to trigger the CoMo to ensure all the signals were received simultaneously.

2.3 Experimental design

The DOE method was used to systematically investigate the relationship between machine parameters, process conditions and micro/nano feature replication height. Five machine process parameters were selected: injection speed (V_i), holding pressure (P_h), holding time (t_h), barrel temperature (T_b) and mold temperature (T_m). The levels of parameters were selected from the preliminary trials, as shown in Table1. In view of the experimental cost, a two level, half factorial 16 run (2^{5-1}), resolution-V design was constructed in this study, as shown in table 2. Each experimental combination was repeated three times to evaluate process variation.

Table 1. Range of machine parameters settings.

Level	V_i (mm/s)	P_h (MPa)	t_h (s)	T_b(^{o}C)	T_m (^{o}C)
+	450	120	0.6	1[a]	70
–	100	70	0.2	–1[b]	40

[a]High level barrel temperature settings from hopper to nozzle:30, 130, 140, 150, 160 ^{o}C.
[b]Low level barrel temperature settings from hopper to nozzle:30, 130, 135, 140, 150 ^{o}C.

Table 2. Experimental design matrix.

Process conditions	V_i(mm/s)	P_h(MPa)	t_h(s)	T_b(^{o}C)	T_m(^{o}C)
1	–	–	–	–	+
2	+	–	–	–	–
3	–	+	–	–	–
4	+	+	–	–	+
5	–	–	+	–	–
6	+	–	+	–	+
7	–	+	+	–	+
8	+	+	+	–	–
9	–	–	–	+	–
10	+	–	–	+	+
11	–	+	–	+	+
12	+	+	–	+	–

13	–	–	+	+	+
14	+	–	+	+	–
15	–	+	+	+	–
16	+	+	+	+	+

2.4 Shot size optimization

Short shot trials were used to optimize shot size for each process condition. The velocity pressure switchover position of the machine was set at 5mm. The short shot trials started from 7mm in shot size. The increment was 0.02mm and the corresponding volumetric increment was 3.077mm^3.

2.5 Measurement

Each sample for measurement was randomly selected from 30 parts which were molded under the same combination of machine process parameters. The replicated heights of features were measured by a Veeco optical profilometer. A FIB milling technique was used to cut away a section of the features in order to observe the profile of the features. A Pt strip layer was deposited via e-beam across the ridges and channels to protect the feature integrity during the FIB milling process. A rectangular section was cut directly in front of the deposited Pt layer. According to Volker et al [27], the temperature increase could be estimated by

$$T = \frac{P}{\pi a k} \tag{1}$$

where P is beam power, a is beam radius and k is thermal conductivity of the substrate during FIB milling process. For our case, the beam voltage is 3.0kV and beam current is 1nA during the milling process. The beam radius is around 80nm. The thermal conductivity is around 0.5 W/mK for HDPE. Therefore, the temperature increase can be estimated as 24 ^{o}C. Because the FIB milling process is carried out at room temperature, the substrate temperature was estimated to reach around 50 ^{o}C during milling, which is significantly lower than HDPE peak melting temperature (130 ^{o}C). In addition, Pt is a good thermal conductor, which also would help deliver the heat during milling process. Therefore, the features would not melt during the milling process. For ridges, the profiles of features are exposed directly, as shown in figure 3 (a). For channels, the profiles of channels can be reflected by cutting though a deposited Pt layer, as shown in figure 3 (b).

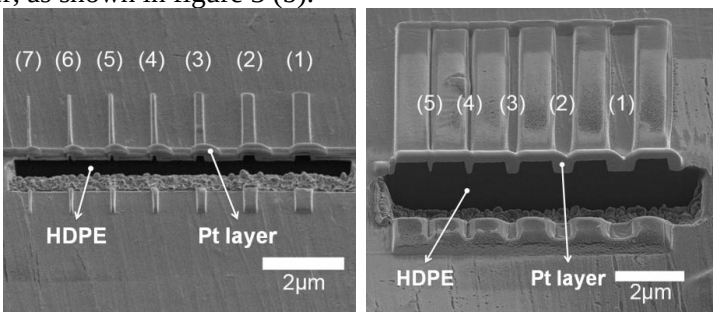

(a) (b)

Figure 3. Cross section of micro/nano features on the molded part machined by FIB milling: (a) ridges, (b) channels.

3. Results and discussion

3.1 Micro and nano-scale feature replication

Figure 4 exhibits the SEM images of ridges and channels replicated by micro injection molding along and against the flow direction (FD), which is illustrated in figure 2 (a) under process condition 16. All the features on the mold insert were well replicated. The minimum feature we have successfully replicated is around 150 nm, which is located on the replicated UCD logo, as shown in figure 4 (e) and (f). In addition, during SEM imaging, a layer of gold

was coated on the surface of polymer to make it conductive. During the imaging process, incoming electrons have high kinetic energy of around 5 to 30 keV, the magnitude of which depends on the acceleration voltage [28]. Most of the kinetic energy of electrons is converted to heat on impingement and both the gold coating and the polymer sample will be heated. Due to the different shrinkage behavior of polymer and gold, the gold layer will show some fine cracks, as shown in figure 4 (f).

It can be seen that ridges along the flow direction have a better replication quality than those against the flow direction, especially for smaller features, as shown in figure 4 (a) and (c). Instead, channels along the flow direction have similar replication quality to those against the flow direction, as can be observed from figure 4 (b) and (d). In order to gain further insight into the replication quality of micro channels and ridges, the FIB milling technique was used to expose the profile of micro/nano channels and ridges, as shown in figure 3. Each ridge and channel was nominated in sequence from big to small. As shown in figure 5, ridges against the flow direction present round edges and their profile has a trend to incline with the flow direction. Ridges along the flow direction have sharp edges, especially for ridges of width greater than 1μm. Ridges narrower than 1μm width along the flow direction also exhibit bigger replicated heights than those against the flow direction. This indicates that smaller features, especially nano scale features are more sensitive to the flow direction.

The cross-sections of channels along and against the flow direction are displayed in figure 6. It can be seen that the height and profile of channels are similar and no significant difference can be observed. The minimum channel we have successfully replicated is around 0.5μm in width and around 1.7μm in depth.

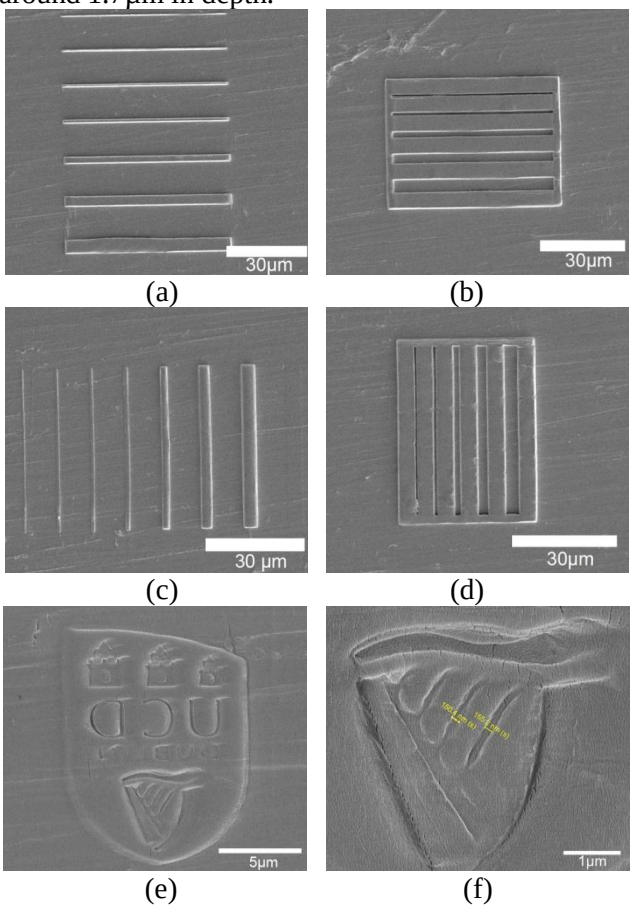

(a) (b) (c) (d) (e) (f)

Figure 4. Top view of replicated micro/nano feature: (a) ridges along flow direction, (b) channels along flow direction, (c) ridges against flow direction,(d) channels against flow direction, (e) replicated nanostructured UCD logo, (f) replication details of UCD logo(the thickness of the channel is around 150nm).

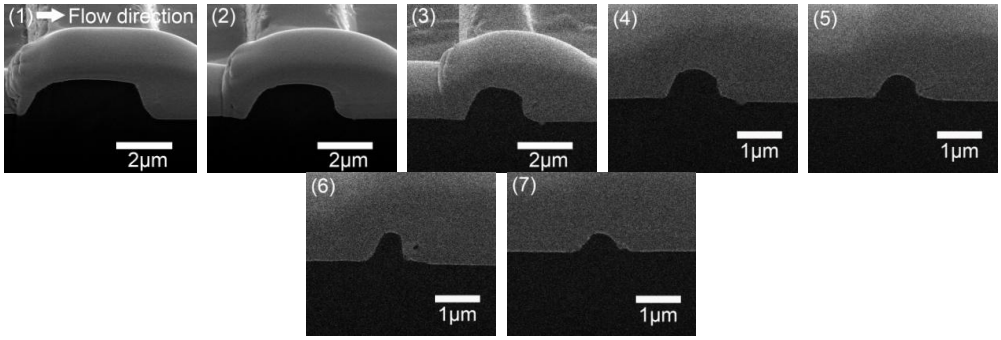

(a)

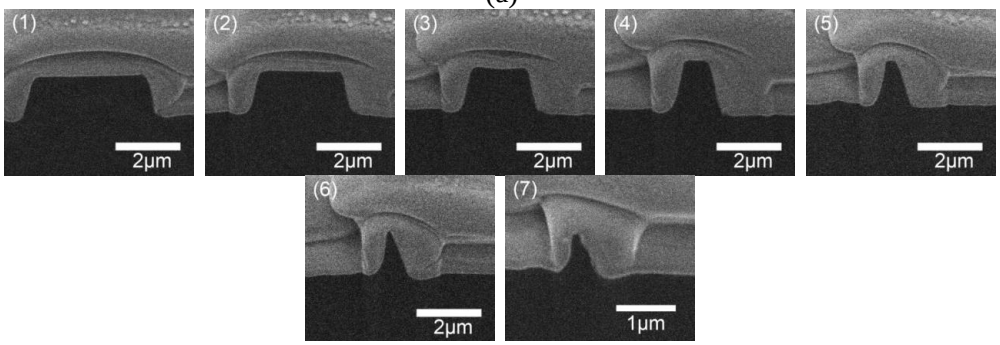

(b)

Figure 5. Profiles of ridge features: (a) against flow direction (b) along flow direction

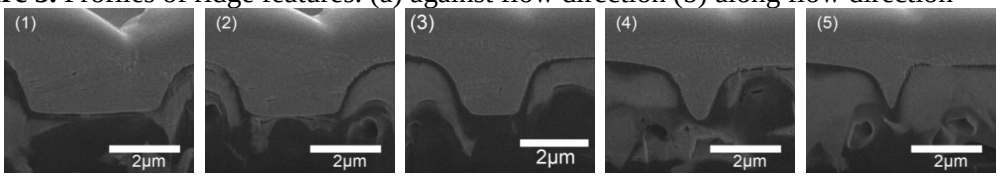

(a)

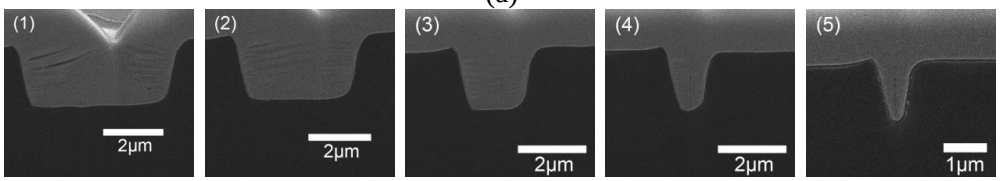

(b)

Figure 6. Profiles of channel features: (a) against flow direction, (b) along flow direction

The width, height and aspect ratio of individual ridges are displayed in figure 8. The replicated height of ridges against the flow direction does not change too much from feature 1 to 3, as shown in figure 7 (a). The maximum aspect ratio is around 1.2, which is achieved by feature 6. For ridges along the flow direction, the replicated height is nearly constant when the width decreases from 4.3 to 0.89 μm from ridge 1 to 5. The maximum aspect ratio is 1.86 for feature 5. As shown in figure 7 (b), the replicated feature height gradually decreases with feature width. It seems to be a critical width available for features both along and against the flow direction under which the replicated height will significantly decrease, as shown in figure 7 (b). The filling percentage of each feature is displayed in figure 7 (c). It is clear that none of are fully filled. The maximum filling we can achieve is around 90%. Similarly, as shown in figure 8, channels along the flow direction have a slight better replication than those against the flow direction and the maximum aspect ratio was 2.8 with a maximum filling percentage of 99%. The depth of channels slowly decreases with channel width. The replication of channels has much less sensitivity to channel width and flow direction compared to ridges.

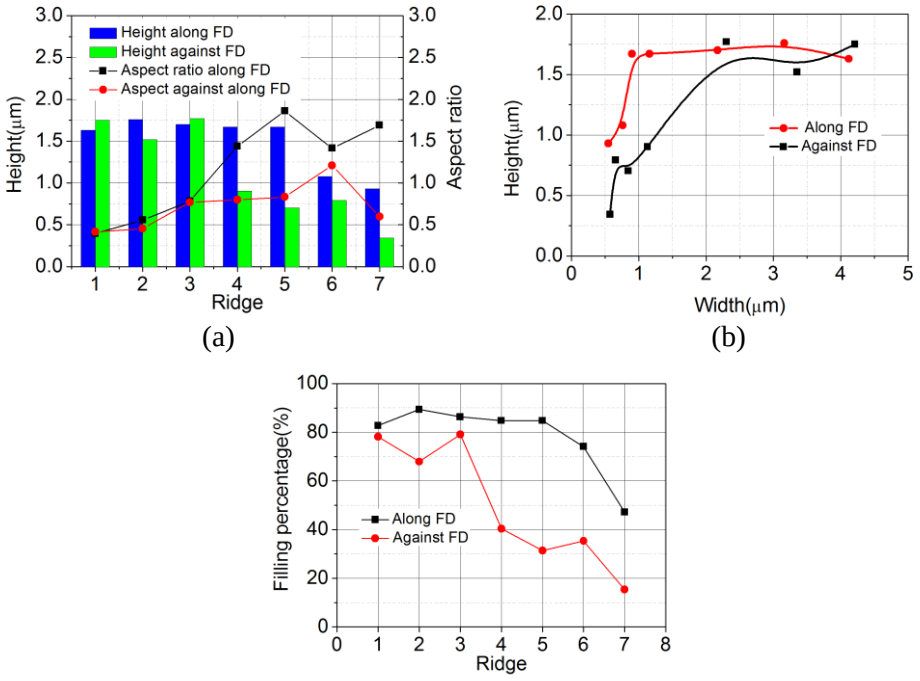

Figure 7. Ridges replication quality: (a) height and aspect ratio, (b) height Vs width, (c) filling percentage.

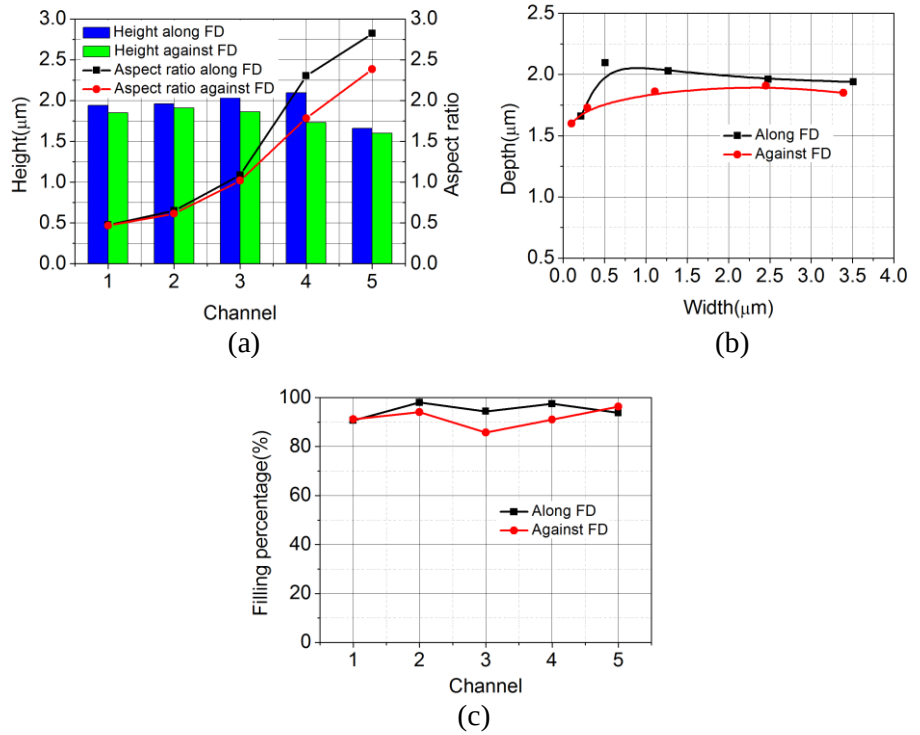

Figure 8. Channel replication quality: (a) height and aspect ratio, (b) depth Vs width, (c) filling percentage.

For features with the same geometrical dimensions, the sensitivity of replicated micro/nano feature to the flow direction of polymer melt could be explained by the phenomenon of air entrapment during filling process. The relative position of a fountain flow front and micro/nano cavity is illustrated in figure 9, where *d* and *h* are the depth and thickness of the micro cavity. Assuming that laminar flow is fully developed in the macro dog-bone cavity and the melt front is a semicircle with radius *R* which is the half thickness of

the cavity (~250μm), the area of patterns, as shown in figure 1(d), is around 200 μm×200μm, which is totally covered by the fountain flow front. This means that the patterns on BMG contact polymer melts almost at the same time. Therefore, the pressure history for ridges along and against the flow direction is almost the same. Temperature distribution is also assumed to be constant on this small pattern region.

As shown in figure 9 (b), the gap δ between the fountain flow front and the edge of the micro cavity can be estimated by

$$\delta = R - \sqrt{R^2 - h^2} \tag{2}$$

Consider ridge 1 as an example: the corresponding length of cavity on the BMG insert along and against the flow direction is 50 μm and 4μm, respectively; the corresponding gaps are around 5μm and 0.05 μm. Clearly most of the air in the micro cavity that is aligned parallel to the flow direction can escape from the cavity during filling. On the other hand, a larger volume of air will be entrapped in the cavity that is aligned against the flow direction: this may prevent further filling of the micro cavity and also affect the profile of micro/nano ridges. In addition, when the melt front reaches the micro/nano feature region of the dog-bone component, the back pressure of the entrapped air against the flow front is estimated to be 0.47MPa based on ideal gas law, which is close to the input cavity pressure for micro/nano features before solidification, which might influence both feature filling distance and its profile. In addition, the profiles of features aligned against the flow direction inclines with flow direction, which might be due to a macro flow field in the dog-bone component for an open type cavity flow [29]. This physical explanation of sensitivity of micro/nano feature to flow direction is consistent with simulations that have been made of micro scale features [30].

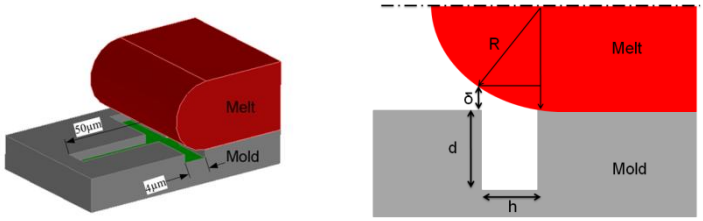

(a) (b)

Figure 9. Schematic representation of advancing front and micro/nano cavity: (a) 3D view, (b) 2D view.

However, the replication quality of micro/nano channels is less sensitive to the flow direction. This can be explained by the fact that the ridges on the mold insert are located in a negative cavity which is bigger than the ridge itself and air could escape from side channels of the negative mold, when the feature is oriented against the flow direction as shown in figure 2 (d). Another possible reason is that the filling spacing between ridges in the negative BMG mold cavity is 5 μm (c.f. figure 2 (c) and (d)), which is big enough to contain the air, making the effect from entrapped air insignificant.

3.2 Relationship between machine process parameters and process characteristic values

In the present study, efforts were made to control the replication quality of the micro/nano features by in-line monitoring of the cavity pressure and temperature. Figure 10 displays the trace curve of injection pressure, cavity pressure and temperature within 1.0s of a production cycle. Peak cavity pressure and peak material contact temperature were selected as process characteristic values to represent the actual cavity pressure and temperature history during the injection molding process.

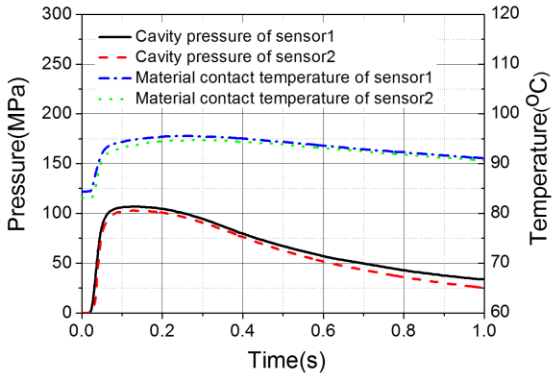

Figure 10. Profile of injection pressure, cavity pressure and temperature within1.0s.

We used statistical analysis to elucidate the effect of machine parameters on peak cavity pressure of sensor1 and sensor2 ($P_{1,max}$, $P_{2,max}$), and peak material contact temperature of sensor1 and sensor2 ($T_{1,max}$, $T_{2,max}$). We assigned PT sensor nearest the gate as sensor1 and the one furthest from the gate as sensor2, as illustrated in figure 1 (b). As shown in figure 11, holding pressure has the most significant effect on peak cavity pressure. Both barrel temperature and mold temperature have a positive effect on peak cavity pressure, which can be explained by the P-v-T behavior of material. Mold temperature has the predominant effect on the material contact temperature. The interactions of machine parameters are insignificant.

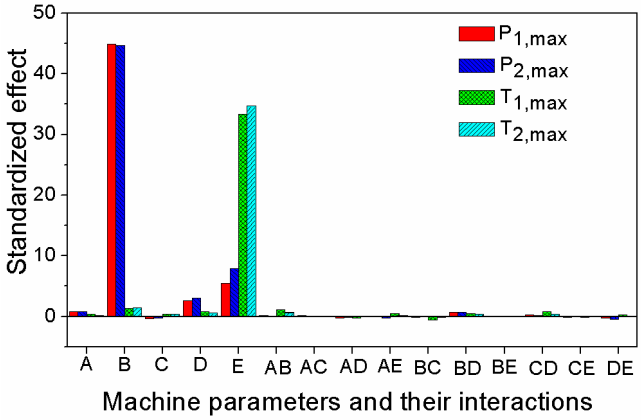

Figure11. Effect of machine parameters on peak injection pressure, cavity pressure and material contact temperature (Parameters A=V_i, B=P_h, C=t_h, D=T_b, E=T_m (c.f. Table1)).

3.3 Relationship between process characteristic values and replication qualities

The mean height of ridge 3 was selected to indicate the quality of replication under different process conditions. The measured height with different process conditions was shown in figure 12. It can be seen that the ridge height presents a significant response to machine parameters. Further, features with lower mean height show relatively high standard deviation; this might be due to process variations and insufficient capability of the optical measuring system.

The trend of replicated height with peak cavity pressure and temperature is also displayed in figure 12. It is obvious that the height presents a positive response to both cavity pressure and temperature. Also, the variation of height is determined by both the pressure and temperature together. For example, when the cavity pressure is higher and the cavity temperature is lower for case 3, in which they are both of positive slopes, the response of the feature height is also of positive slope. The same trend can be seen for case 6, in which cavity pressure is lower and temperature is higher, but they are both of positive slopes; the net result is that the feature height increases for positive slope. The difference between case 3 and case 6 is that height is lower for case 3 than for case 6 due to the higher pressure and lower

temperature. This indicates that temperature has a more significant effect on replicated height than pressure. The same observation can also be found in other cases.

Figure 13 exhibits the statistical distribution of the height of ridge 3 with peak cavity temperature and peak cavity pressure as monitored by sensor1. It can be seen that the best distribution zone is within the temperature range of 77~95^{o}C and 65~110MPa in pressure. Increasing both cavity temperature and cavity pressure within a certain range can enhance filling of features. For example, when the peak cavity temperature is 85^{o}C, the feature height increases with peak cavity pressure when pressure is less than 75MPa. Similarly, further filling of features can be achieved when peak temperature is lower than 78^{o}C at a fixed peak cavity pressure 75MPa. This illustrates that continuing to increase of cavity pressure and temperature beyond a certain value will not give further filling for micro and nano features. Therefore, we can improve feature replication quality by controlling cavity pressure and temperature with machine parameters and other accessory equipments, such variotherm mold heating systems.

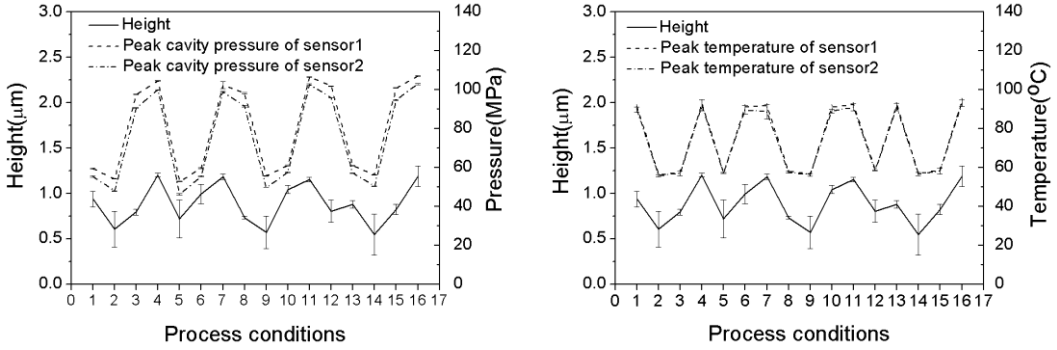

(a) (b)

Figure 12. (a) Peak cavity pressure and height for under different process conditions (c.f. Table 2), (b) Peak material temperature and height under different process conditions.

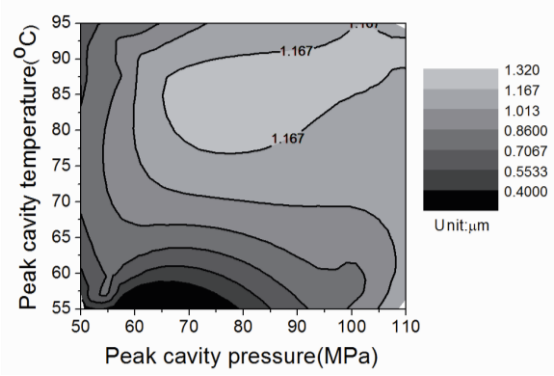

Figure 13. Height distribution with cavity temperature and pressure (Parameters A=V_i, B=P_h, C=t_h, D=T_b, E=T_m (c.f. Table1)).

3.3 Relationship between machine process parameters and feature replication

Statistical analysis shown in figure 14 illustrates the influence of machine parameter settings on the replication height of ridge3. It is clear that holding pressure and mold temperature have the most significant effect on the height of ridge3.

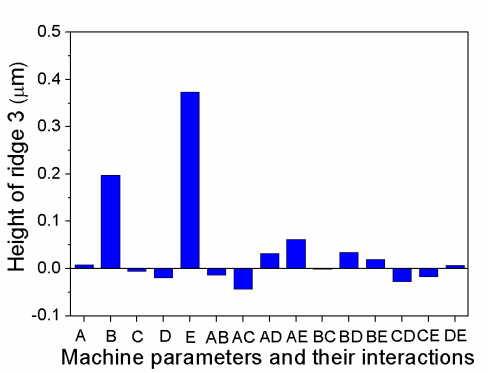

Figure 14. Effect of machine parameters on replicated height of feature3 (Parameters A=V_i, B=P_h, C=t_h, D=T_b, E=T_m (c.f. Table1)).

The filling depth of micro/nano features, as shown in figure 7 (b), can be estimated by a simple pressure driven flow model,

$$d = h\left[\frac{t_f\left(P - P_{capillary} - P_{air}\right)}{12\eta}\right]^{1/2} \tag{3}$$

where d is filling depth, P is pressure at entrance of micro/nano cavity, h is feature wall thickness, t_f is the filling time, $P_{capillary}$ is capillary pressure induced by surface tension, P_{air} is entrapped air pressure inside of cavity, η is average viscosity.

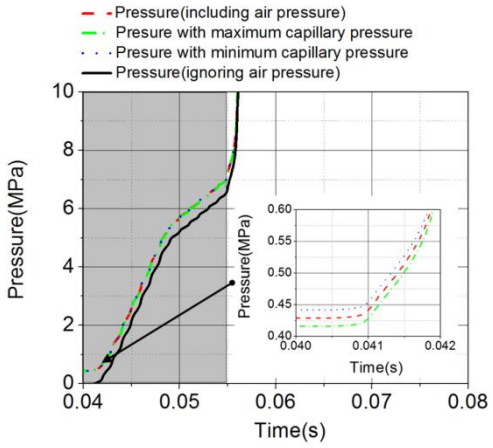

Figure 15. Input pressure during micro/nano feature filling process

Capillary pressure induced by surface tension [31] can be calculated by

$$P_{surface} = -\frac{2\gamma\cos\theta}{h} \tag{4}$$

where channel length $l >> h$, γ is surface tension of polymer melts, which is around 25mN/m[32] for HDPE, θ is dynamic contact angle between polymer melts and mold. The pressure of entrapped air can be estimated by ideal gas law in an adiabatic process [33],

$$P_{air} = P_1\left(\frac{V_1}{V_2}\right)^y \tag{5}$$

where P_1, V_1 are initial state values and P_{air}, V_2 is current state values, y is a constant which is 7/5 for a diatomic gas such as nitrogen and oxygen. In our case, the initial volume is assumed to be the dog-bone component V_1=25.34mm^3 and the initial pressure is assumed to be ambient pressure P_1=0.101MPa. V_2 is approximated by the rest of volume when the melt front strikes sensor 2, which is around 8.34mm^3. The air pressure could be estimated as 0.47MPa. Figure 15 displays the input pressure in the micro/nano features regions, which is approximated both by pressure of sensor 2, air pressure and capillary pressure. It can be seen that the entrapped air pressure has a significant effect on input pressure during 15ms when the

polymer melts contacts micro/nano regions. Capillary pressure has no effect on input pressure. However, when feature thickness is of nanometer scales, capillary pressure will reach the same order of magnitude of cavity pressure and entrapped air pressure, as shown in figure 16.

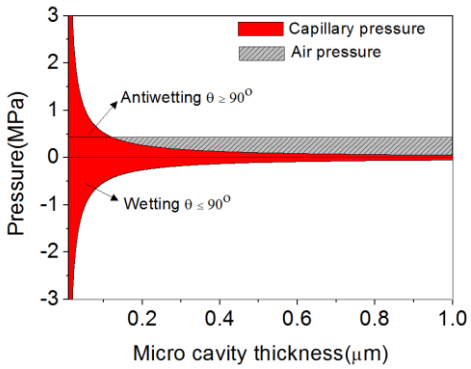

Figure 16. Capillary force Vs micro cavity thickness for HDPE.

The filling time of micro/nano feature can be estimated based on one-dimensional heat conduction [34, 35],

$$t_f = \frac{h^2}{\pi^2 \alpha} \ln\left[\frac{8}{\pi^2}\left(\frac{T_i - T_w}{T_s - T_w}\right)\right] \tag{6}$$

where α is the thermal diffusivity of polymer and T_i is melt temperature, T_w is the cavity wall temperature and T_s is solidification temperature. Figure 15 plots the solidification time verse wall thickness and temperature of micro features for HDPE part, in which α=1.57×10^{-7}m^2/s, T_i = 160^{o}C and T_s = 130 ^{o}C. It can be seen that cavity surface temperature has a prominent effect on the filling time of micro/nano features. The increase of mold temperature could remarkably elevate cavity wall temperature, which will extend micro cavity filling time. For figure 1 with cavity thickness of 4μm, the estimated filling time is around 3μs when the mold wall temperature was 83^{o}C, as suggested in figure 17(b).

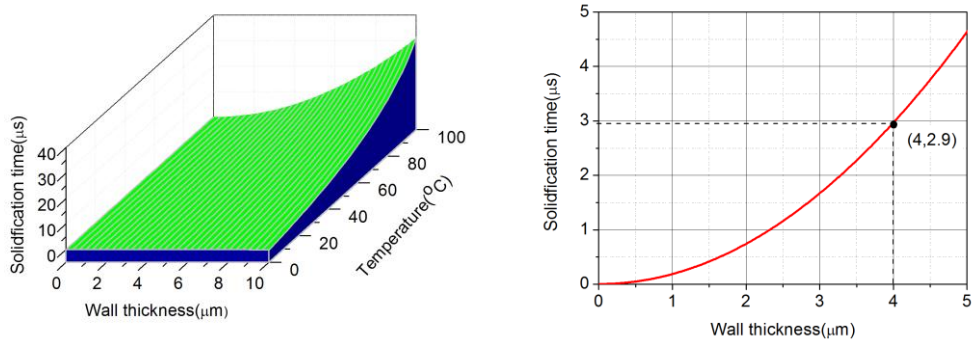

(a) (b)

Figure 17. Estimated solidification time: (a) time Vs feature thickness and mold wall temperature, (b) time Vs wall thickness at cavity wall temperature T_w =83^{o}C.

In addition, creep deformation of the frozen layer could also help the replication of channels after solidification. According to Yoshii's transcription model[36], the deformation of the frozen layer during post filling of micro/nano features can be estimated by a simple beam bending model,

$$d \sim \frac{Ph^4}{32EH^3} \tag{7}$$

where P is cavity pressure, h is feature wall thickness, E is modulus of elasticity of HDPE at cavity wall temperature, H is thickness of frozen layer. It is known that the modulus E of HDPE is gradually decreases with temperature. Based on a two phase Stefan problem and approximation of Lambda [37, 38], the frozen thickness of HDPE during the molding process

can be estimated and shown in figure 18. It is clear that the thickness of the frozen layer will reduce with elevated mold temperature and will logarithmically increase with time. For a feature with fixed geometries, the bending flexibility is proportional to cavity pressure and of minus third powers of thickness of frozen layer. Therefore, increasing cavity pressure as soon as possible during post filling of micro/nano features could help to further improve the replication of features.

Therefore, the replication of micro/nano features is closely related to the thermal mechanical history of polymer during the injection molding process. In our previous work [39], we found that both injection velocity and holding pressure have a significant effect on the average cavity pressure and average cavity filling velocity during the filling process of a dog-bone component, because of the earlier transition from velocity control in injection stage to pressure control in holding stage. This will increase the cavity pressure and decrease the melt viscosity. However, statistical analysis suggests that injection velocity has no significant effect on micro/nano feature filling. This suggests that creep deformation may play a more important role in the filling of micro/nano features.

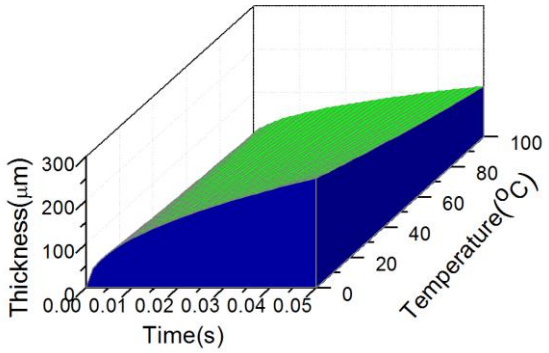

Figure 18. Estimated frozen layer thickness Vs time and mold wall temperature.

3.3 Wear of bulk metallic glass material during molding process

The BMG mold insert was examined by SEM after around 10,000 and 20,000 molding cycles in order to inspect any surface wear and the integrity of micro/nano scale features. Generally, many studies has been carried out to explore the sliding and wear behavior of amorphous alloys, which have been summarized in an excellent review by Greer et al [40]. Wear of BMG was also found in the present study when using BMG as a micro/nano feature insert. When we compare the surface conditions of the BMG tool before use (c.f. figure 2) and after around 10,000 cycles (c.f. figure 19), we can find a number of new scratches on the surface, excluding the machining marks. Comparing figure 2 (d) and figure 19 (b), the micro/nano features actually retain their shape without any significant cracking, except for some local contamination. In order to remove these impurities, acetone was used to clean the surface of the BMG insert in an ultrasonic bath; this could have led to some pitting defects. However, after around 20,000 cycles, the features cracked. The remaining features appear to be aligned with the flow direction of the polymer melt. In addition, the relatively smaller features retain less of their volume than do the bigger features. From the perspective of flat surfaces, we can observe relatively deeper scratches after 20,000 cycles, as shown in figures 19 (c) and (d). These could have been either caused by accidentally breaking the molded parts during the de-molding process in several materials experiments, such as COC or wear of BMG during such many cycles. The roughness of the BMG insert, as shown in figure 20, increases by 5.6%, 5%, 3.9% and 3.9% respectively for R_a, R_q, R_z and R_t.

It is well known that injection molding is a repeating process. The high temperature polymer melt is injected into the mold and solidifies to form a part. The mold materials will experience fluctuations ranging from high temperature (melt temperature) to relatively low temperature (mold temperature) during the molding process. For the present micro injection molding experiment, due to the high surface to volume ratio for both micro dog-bone

components and micro/nano features, high injection speeds and pressures were exerted on polymer melt in the cavity. As a result, the BMG endured higher shear stress and temperature than in conventional injection molding. In addition, various other plastics, including PP, POM, COC, PMMA, PC, Pebax, etc, were used as molding materials during trials and other experiments, which would have provided different electrochemical environments at diverse pressures and temperatures, in which the maximum temperature reached 300^{o}C. Although the working temperature of BMG is higher than room temperature and can even reach 300^{o}C when processing some plastic materials (e.g., polycarbonate), it was still below the Tg (glass transition temperature) of the present BMG (Tg=435^{o}C). Therefore, the BMG would have experienced an annealing process for every molding cycle. This associated annealing could have induced structure relaxation and, in turn, embrittlement of the BMG [41]. This would serve to decrease the material's wear resistance, especially under abrasive conditions, although this point is still controversial [40].

Fatigue of BMG could be the main reason for the observed wear and cracking of the micro/nano features of BMG. Structural components are frequently subjected to repeated or cyclic loading. The resulting cyclic stresses, which may be far below the ultimate tensile strength of materials, can result in a microscopic physical damage to the material. The microscopic damage can accumulate with continued cyclic loading until it develops into a crack that could lead to the catastrophic failure. This process of damage and failure due to cyclic loading is fatigue [42] and the effects can vary depending on size of the BMG part [43]. High temperature and repeated annealing could be possible reasons that would enhance this process. For micro/nano features, FIB irradiation can induce a change in density and may introduce a nanocrystalline structure, depending on the irradiation conditions [44-46]. However, the dimensions of such a formed nanocrystalline structure would be around 10nm [45, 46]; this would not improve the wear resistance of the BMG because the crystal size is too small to support normal loads [40]. In addition, the size effect may be taken into account when considering the fatigue behavior of micro/nano features.

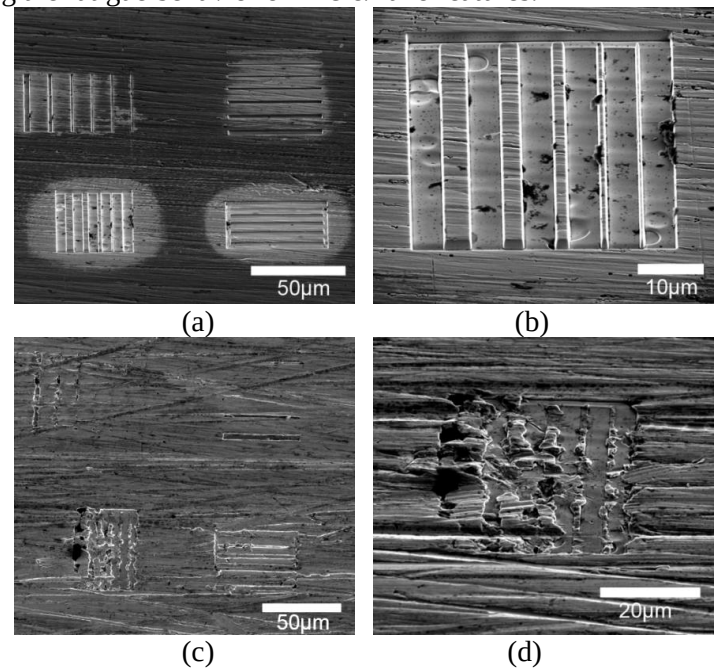

Figure 19. Micro/nano scale feature on BMG insert: (a) plan view after around 10000 cycles (b) ridges after around 10000 cycles (c) plan view after more than 20000 cycles (d) ridges after more than 20000 cycles.

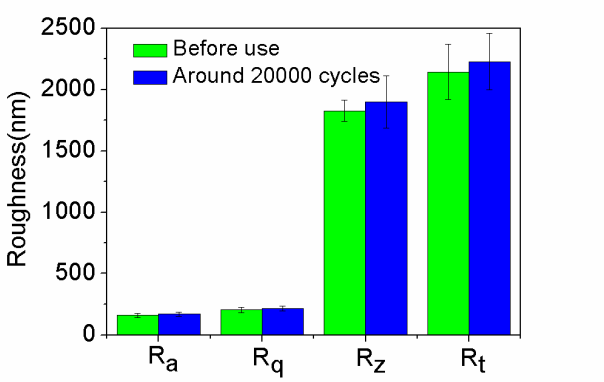

Figure 20. Surface roughness of BMG insert before use and after around 20000 cycles.

4. Conclusions

In this study, micro/nano scale ridges, channels and nanostructured surfaces were well replicated with the micro injection molding process by using a BMG insert. The minimum feature we can replicate is around 150nm and the micro/nano ridges and channels we can successfully replicate range from 4μm to 300nm, with the maximum aspect ratio being 2.8. The experiments reveal that the quality of micro/nano features is very sensitive to the flow direction. The ridges that are oriented against the flow direction have round edges and their profiles are inclined with the flow direction. On the other hand, ridges that are aligned along the flow direction have sharp edges and better replicated heights. Channels exhibit fewer significant differences than ridges. The sensitivity of feature replication to the flow direction can possibly be explained by a proposed entrapped air model. In addition, the filling of features decreases with their width, especially for sub-micron features. Consequently, the well designed of features and their configurations are of great importance for replication.

According to the in-line measurement of real cavity pressure and temperature and the statistical analysis on machine parameters, real process conditions and replicated quality, it can be seen that the holding pressure, melt temperature and molding temperature have a positive effect on cavity pressure and temperature; the filling of micro features can be improved by increasing cavity pressure and temperature within a certain range; high holding pressure and high temperature can help with filling of micro/nano features. Consequently, based on the proposed simple pressure driven flow model and beam bending model, we concluded that the thermomechanical history that polymer experiences during both melts filling and frozen layer creep deformation of post-filling will determine the forming of micro/nano features. Statistical analysis indicates that the creep deformation may play a more important role in forming micro/nano features.

The loss of features on the BMG insert was analyzed simply by observing the surface condition of the insert after around 10,000 molding cycles and more than 20,000 cycles. The results indicate that BMG can preserve the integrity of features for around 10,000 molding cycles, but the integrity can be destroyed after more than 20,000 cycles. This fatigue behavior of micro/nano features of a BMG tool under high temperature and repeated annealing merits further investigation.

Acknowledgments

The authors gratefully acknowledge financial support from Chinese Scholarship Council and University College Dublin and Enterprise Ireland (Grant No. CFTD/07/314 & CFTD/06/IT/335).

References

[1] Giboz J, Copponnex T and Mélé P 2007 Microinjection molding of thermoplastic polymers: a review *J. Micromech. Microeng.* **17** 96–109

[2] Haeberle S and Zengerle R 2007 Microfluidic platforms for lab-on-a-chip applications, *Lab on a Chip* **7** 1094–110

[3] Abgrall P and Gué A-M 2007 Lab-on-chip technologies: making a microfluidic network and coupling it into a complete microsystem— a review *J. Micromech. Microeng.***17** 15–49

[4] Craighead H 2006 Future lab-on-a-chip technologies for interrogating individual molecules *Nature* **442** 387–93

[5] Cannon D M, Flachsbart B R, Shannon M A, Sweedler J V and Bohn P W 2004 Fabrication of single nanofluidic channels in poly(methylmethacrylate) films via focused-ion beam milling for use as molecular gates *Appl. Phys. Lett.* **85** 1241–3

[6] Lee C H, Jung P G, Lee S M, Park S H, Shin B S, Kim J H, Hwang K Y, Kim K M and Ko J S 2010 Replication of polyethylene nano-micro hierarchical structures using ultrasonic forming *J. Micromech. Microeng.* **20** 035018

[7] Yoo Y E, Kim T H, Choi D S, Hyun S M, Lee H J, Lee K H, Kim S K, Kim B H, Seo Y H and Lee H G 2009 Injection molding of a nanostructured plate and measurement of its surface properties *Current Applied Physics* **9** 12–8

[8] Ito H, Suzuki H, Kazama K, and Kikutani T 2009 Polymer structure and properties in micro- and nanomolding process *Current Applied Physics* **9** 19–24

[9] Becker H and Gärtner C 2000 Polymer microfabrication methods for microfluidic analytical applications *Electrophoresis* **21** 12–26

[10] Heckele M, and Schomburg W K, 2004, Review on micro molding of thermoplastic polymers, *J. Micromech. Microeng.* **14** 96–109

[11] Kamal M R, Chu J S, Derdouri S and Hrymak A 2010 Morphology of microinjection molded polyoxymethylene *Plast Rubber Compos* **39** 332–41

[12] Whiteside B R, Spares R, Howell K, Martyn M T and Coates P D 2005 Micromolding: extreme process monitoring and inline product assessment *Plast. Rubber. Compos* **34** 380–6

[13] Chu J S, Kamal M R, Derdouri S and Hrymak A, 2010 Characterization of the microinjection molding process *Polym. Eng. Sci*. **50** 1214–25

[14] Barbero D R, Saifullah M S M, Hoffmann P, Mathieu H J, Anderson D, Jones G A C, Welland M E and Steiner U 2007 High resolution nanoimprinting with a robust and reusable polymer mold *Adv. Funct. Mater.* **17** 2419–25

[15] Zankovych S, Hoffmann T, Seekamp J, Bruch J U and Torres C M S Nanoimprint lithography: challenges and prospects. *Nanotechnology* **12**, 91–5

[16] Kumar G, Tang H X and Schroers J 2009 Nanomolding with amorphous metals *Nature* **457** 868-72

[17] Pan C T, Wu T T, Chen M F, Chang Y C, Lee C J and Huang J C 2008 Hot embossing of micro-lens array on bulk metallic glass *Sensors And Actuators* **141** 422–31

[18] Henann, D L, Srivastava V, Taylor H K, Hale R M, Hardt E D, and Anand L 2009 Metallic glasses: viable tool materials for the production of surface microstructures in amorphous polymers by micro-hot-embossing *J. Micromech. Microeng.* **19** 115030.

[19] Stratton D J, Byrne C, Mulcahy J and Browne D J, 2011 Sub-micron feature patterning of thermoplastics using multi-scale BMG Tooling *Materials Research Society Proceedings* **1300** mrsf10-1300-u02-08

[20] Fu G, Tor S B, Loh N H and Hardt D E 2010 Fabrication of robust tooling for mass production of polymeric microfluidic devices *J. Micromech. Microeng.* **20** 085019

[21]Zhang N, Browne D J and Gilchrist M D 2011 *Effect of design on the replication of micro/nano scale features in the micro injection molding process: Proceedings of the 8th International Conference on Multi-Material Micro Manufacture (Stuttgart, Germany)(Research Publishing)* ed H Kück, H Reinecke and S Dimov pp 68-73.

[22] Pryds, N H. 2004 Bulk amorphous Mg-based alloys *Materials Science and Engineering A* **377** 186-93

[23] Chu J P, Wijaya H, Wu C W, Tsai T R, Wei C, Nieh T G, and Wadsworth J 2007 Nanoimprint of gratings on a bulk metallic glass *Applied Physics Letters* **90** 034101.

[24] Schroers J 2010 Processing of bulk metallic glass *Advanced materials* **22** 1566-97

[25] Brousseau E B, Dimov S S, and Pham D T 2009 Some recent advances in multi-material micro- and nano-manufacturing *The International Journal of Advanced Manufacturing Technology* **47** 161-80

[26] Zhang N, Byrne C J, Browne D J and Gilchrist M D 2012 Towards nano-injection molding using metallic glass tools *Materials Today* In press.
[27] Volkert C A and Minor A M 2007 Focused Ion Beam Microscopy and Micromachining *MRS BULLETIN* **32** 389–95.
[28] Hwang, IL-han, Suck-joo Na 2005 A Study on Heat Source Modeling of Scanning Electron Microscopy Modified for Material Processing *Metallurgical and Materials Transactions B* **36** 133-39.
[29] Zhang B J, Orishita E M, Kunuki T O and Toh H I 2002 Experimental investigation on the mechanism of flow-type changes in super ultrasonic flows *Trans. Japan Soc. Aero. Space Sci.* **45**170-9
[30] Tada K, Fukuzawa D, Watanabe A and Ito H 2010 Numerical simulation for flow behaviour on micro- and nanomolding *Plastics, Rubber and Composites* **39** 321–6
[31] Kim D S, Lee K C, Kwon T H and Lee S S, 2002 Micro-channel filling flow considering surface tension effect *J. Micromech.Microeng.* **12** 236–46
[32] Yang D, Xu Z, Liu C and Wang L 2010 Experimental study on the surface characteristics of polymer melts *Colloids and Surfaces A: Physicochemical and Engineering Aspects* **367** 174–80
[33] Griffiths C A , Dimov S S, Scholz S, and Tosello G 2011 Cavity air flow behavior during filling in microinjection molding *Journal of Manufacturing Science and Engineering* **133** 011006
[34] Yao D. and Kim B 2002 Simulation of the filling process in micro channels for polymeric materials *J. Micromech.Microeng*. **12** 604–10
[35] Liang J 1996 The calculation of cooling time in injection molding *Journal of Materials Processing Technology* **57** 62-4
[36] Yoshii M, Kuramoto H, and Kato K 1994 Experimental study of transcription of minute width grooves in injection molding *Polymer Engineering and Science* **34** 1211–8
[37] Bai Y, Yin B, Fu X R, and Yang M B 2006 Heat transfer in injection molding of crystalline plastics *Journal of Applied Polymer Science* **102** 2249–53.
[38] Hu H, and Argyropoulos S A 1996 Mathematical modeling of solidification and melting: a review *Modelling Simul. Mater. Sci. Eng*. **4** 371–96.
[39] Zhang N, Chu J and Gilchrist M D 2011 Micro injection molding: characterization of cavity filling process *Proceedings of SPE Annual Technical Conference* pp 2085–91.
[40] Greer A L, Rutherford K L, and Hutchings I M 2002 Wear resistance of amorphous alloys and related materials *International Materials Reviews* **47** 87-112.
[41] Kumar G, Rector D, Conner R D, and Schroers J 2009 Embrittlement of Zr-based bulk metallic glasses *Acta Materialia* **57** 3572-83.
[42] Wang G and Liaw P K 2008 *Bulk metallic glass: an overview* ed. Miller M, Liaw P (New York: Springer) p169.
[43] Wang G Y, Liaw P K, Yokoyama Y, and Inoue A 2011 Size effects on the fatigue behavior of bulk metallic glasses *Journal of applied physics* **110** 113507.
[44] Noritaka K , Morita N, Yamada S, Takano N, Oyama T, Ashida K, Momota S, Taniguchi J, Miyamoto I, and Ofune H 2007 Sub-micrometer-scale patterning on Zr-based metallic glass using focused ion beam irradiation and chemical etching *Nanotechnology* **18** 375302.
[45] Nagase T, and Umakoshi Y 2004 Electron irradiation induced crystallization of the amorphous phase in $Zr_{65.0}$ $Al_{7.5}$ $Ni_{10.0}$ $Cu_{17.5}$ metallic glass *Science and Technology of Advanced Materials* **5** 57-67.
[46] Tarumi R, Takashima K, and Higo Y 2002 Formation of oriented nanocrystals in an amorphous alloy by focused-ion-beam irradiation. *Applied Physics Letters* **81** 4610-12.